Energy redistribution patterns in damaged elastic frames

Energy redistribution patterns in damaged elastic frames☆

Valerio De Biagi[a,b]

[a] *Dept. of Structural, Geotechnical and Building Engineering, Politecnico di Torino, Corso Duca degli Abruzzi 24, Torino 10129 Italy*
[b] *SISCON Centre for the Safety of Infrastructures and Structures, Politecnico di Torino, Corso Duca degli Abruzzi 24, Torino 10129 Italy*

Abstract

Frames structures are systems made of connected elements and are widely diffused in civil and industrial engineering. Like other structural types, they can suffer damages. Element removal can cause the collapse of the whole structure. Alternate load path is a strategy to prevent collapse through the redistribution of the forces to the safe elements. Although this approach is largely adopted in the design of robust structures, the knowledge on how the redistribution mechanism act is still limited. To understand the mechanisms that raise, the strain energy in each structural component is considered as indicator. Two dimensionless quantities, i.e., beam-to-column flexural stiffnesses and transposed-to-proper column inertia are found to be the two relevant terms that rule the patterns of strain energy on the damaged frame. A relationship between the patterns, the increment of energy and the two dimensionless quantities is found, providing interesting insights into the behavior of such statically indeterminate structure. The results can be used for new approaches to robustness-oriented structural design.

Keywords: frame structure, internal energy, damage, energy pattern, parameters

1. Introduction

Frame structures are systems of elements, namely beams and columns, that are joined together to form an assembly. Such types of structures are able to carry the loads applied on them since moment-resisting mechanisms develop. From a statical point of view, the frames are statically indeterminate structures with a high degree of indeterminacy. Due to their stiffness to vertical and lateral loads, they are largely diffused in all fields of construction engineering, either civil or mechanical [1, 2, 3]. Frames structures are found at a wide range of scales and artifacts: from tall buildings [4, 5], to medium component scale [6, 7], to material scale [8, 9], from aircraft [10] to ship engineering [11]. They are largely adopted in addictive manufacturing for highly engineered materials [12, 13]. Although they are in man-made products, there are examples of frame structures in Nature [14].

As all the other structures, frames can suffer damages. The causes of the major collapses of frame structures encompasses explosions (Murrah Federal Building, Oklahoma City [15]), impacts (World Trade Center, NYC [16]), fire (Plasco Building, Teheran [17]) or overloads (Sampoong Dept. Store, Seoul [18]). The failure of frame structures represents a major concern in civil engineering since such structural types are largely diffused. Thus, their behavior after the removal of one element has been studied with the special purpose to assess the robustness of the structure under all the possible loading scenario that can occur [19, 20]. The majority of such analyses have been performed using numerical softwares, which are able to model material behavior [21], as well to account for the interaction between the elements [22, 23]. Although complete, such analyses lack of generality, since working examples are proposed, e.g., in [24, 25, 26]. Moreover, the collapse response largely differs depending on the type of numerical model adopted for the analysis [26]. Studies on damaged frame structures also include two main problems: damage detection and damage assessment [27]. To this aim, many approaches have been implemented, including machine learning techniques and artificial intelligence [28, 29]. Theoretical studies on the robustness of frame structures subjected to column removal are oriented towards the dynamic effects that originates from the sudden element removal [30, 31], to interpret the results of experiments [32] and to progressive collapse mechanisms [33, 34, 35, 36].

Limited studies on energy aspects on damaged frame structures have been found in the literature. In the Eighties, Sih and Hartranft [37] formulated a preliminary study on the possibility of applying fracture mechanics for the study of the failure of frame structures. Briefly, they argued that the kinetic energy released from the removal of one member cause the failure of the system to proceed and, thus, a progressive collapse occurs. This idea was later explored by Masoero and colleagues [38, 39, 40] who discussed about the analogies between the failure of a frame and fracture mechanics finding scaling laws and ductile-brittle transition in the process. A previous study by the Author on a connected structure made of members with linear elastic material law illustrates that progressive element removal through a simple damage model [41] follows a nonlinear structural response [42]. As highlighted in the study of simplified schemes [43], this is due to the static indeterminacy of the structural scheme and the presence of preferential load paths

☆Author's accepted manuscript in the International Journal of Mechanical Sciences

Email address: valerio.debiagi@polito.it (Valerio De Biagi)

that drive the overall behavior [44]. Unusual strain energy behaviors have been recently observed and detailed by Karpov and colleagues [45, 46]: they studied periodic and lattice metamaterials subjected to localized loads finding that anomalous patterns originates within the structure to distribute the force applied on the boundary.

In frame structures, when an element is removed the loads carried by it are redistributed to the safe elements, usually the adjacent members. Alternate Load Path (ALP) is a strategy widely used in the design of robust structures: when a damage occurs, the loads are rerouted to other elements [47]. Frame structures, thanks to their moment resisting capacity, are able to perform such redistribution [48]. Nevertheless, comparing the undamaged and the damaged schemes, one cannot pinpoint the changes since the elements are subjected to a multitude of forces (two shear forces, one axial force, two bending moments and one torsional moment). Thus, as already proposed by the Author, the internal energy is selected as unique parameter able to summarize the behavior of the structure [44]. The aim of this paper is to highlight how the internal energy is redistributed within the safe structure after element removal. This would serve for a better understanding of frame behaviors and, possibly, for a robustness-oriented structural design.

To this purpose, a discussion following Sih and Hartranft [37] on the energy increments due to element removal in frames structures is first proposed and enriched. Then, dimensionless quantities that describe the geometry and the distribution of the stiffnesses on the scheme are determined thanks to an example on a simple structure. The patterns that originate on a frame structure subjected to element removal are discussed with reference to four possible damage locations. Finally, the results are discussed and the similarities between the determined patterns and the total energy increments are highlighted.

2. Energy aspects in element removal

The well recognized practice in simulating element removal in structures consist in the following four steps [49, 50]. Figure 1 illustrates the process on a simple plane structure subjected to column removal.

1. Solve the undamaged system and get the internal forces at the ends of the element to be removed (Figure 1.a).
2. Create a novel system made of two components: a system (namely, Structure 1, $\mathcal{S}_1$) without the element to be removed and a system (namely, Structure 2, $\mathcal{S}_2$) represented by the removed element; add as extra nodal forces the internal forces computed at step 1 (Figure 1.b).
3. Apply on the nodes of Structure 1 and Structure 2 progressively increasing forces that are opposite to the ones inserted at step 2 (Figure 1.c).
4. When the opposite forces have the same magnitude as the one of step 2 the element is removed (Figure 1.d).

Some considerations about the internal energy during the element removal process are now discussed, also on the base of the previous studies by Sih and Hartranft [37]. The internal energy in the statically indeterminate structure, i.e., the one considered at the step 1, is named as U_0, where subscript $_0$ relates to the undamaged structural scheme. Referring to Figure 1.a, the term U_0 is the sum of two contributions: U_{01} referring to the energy in the horizontal beam computed from the internal forces (bending moment, axial and shear forces); U_{02} referring to the energy in the vertical element computed in the same way (only axial force is present). Menabrea's theorem, which was initially introduced for solving statically indeterminate structures [51], can provide interesting insights into the removal process.

Referring to step 2, the two created structures $\mathcal{S}_1$ and $\mathcal{S}_2$ with the extra force(s) can be considered equivalent to the undamaged scheme in terms of total internal energy since the internal forces (bending moment, axial and shear forces) are exactly the same. A similar conclusion can be reached considering that two structures are statically determinate (i.e., in equilibrium) and, thus, following Menabrea's theorem [52, 53], the value of N is the one for which the displacement compatibility, i.e., $v_{A_1} = v_{A_2}$, (where v denotes the vertical displacement) holds. In fact, the internal energy has a minimum in correspondence of the true force:

$$\left.\frac{\partial U}{\partial X}\right|_{X=N} = 0, \tag{1}$$

where X is the generic axial force and U is the internal energy. For the previous considerations about the internal forces in $\mathcal{S}_1$ and $\mathcal{S}_2$, $U_1 = U_{01}$ and $U_2 = U_{02}$, where U_1 and U_2 are the internal energies in $\mathcal{S}_1$ and $\mathcal{S}_2$, respectively. Since $U = U_1 + U_2$, recalling Eqn. (1):

$$\left.\frac{\partial (U_1 + U_2)}{\partial X}\right|_{X=N} = \left.\frac{\partial (U_1)}{\partial X}\right|_{X=N} + \left.\frac{\partial (U_2)}{\partial X}\right|_{X=N} = 0. \tag{2}$$

Following Castigliano's second theorem [54], the derivative of the internal energy with respect to a force is the displacement component of the point of application of the force. Considering that downward force and, consequently, downward displacement is positive, it results:

$$-v_{A_1} + v_{A_2} = 0 \qquad \text{for } X = N, \tag{3}$$

which is the compatibility condition previously mentioned.

In the incremental process reported in step 3, the total force on the nodes can be considered as the sum of the contribution of N and λN. Increasing the λN, each structure would remain in equilibrium and, thus, the internal energies would modify. Since the U has a minimum for the internal forces that satisfy the compatibility (following Menabrea's theorem), modifying the forces, the total internal energy would increase, it results that

$$\left.\frac{\partial U}{\partial X}\right|_{X=N-\lambda N} \neq 0, \tag{4}$$

from which it results that $-v_{A_1} + v_{A_2} \neq 0$. This means that the compatibility of the displacements does not hold during progressive removal process.

When the opposite forces reaches the value of N, i.e. $\lambda = 1$, the element is completely removed. The internal energy related to this step is named as U_d, where subscript $_d$ stands for

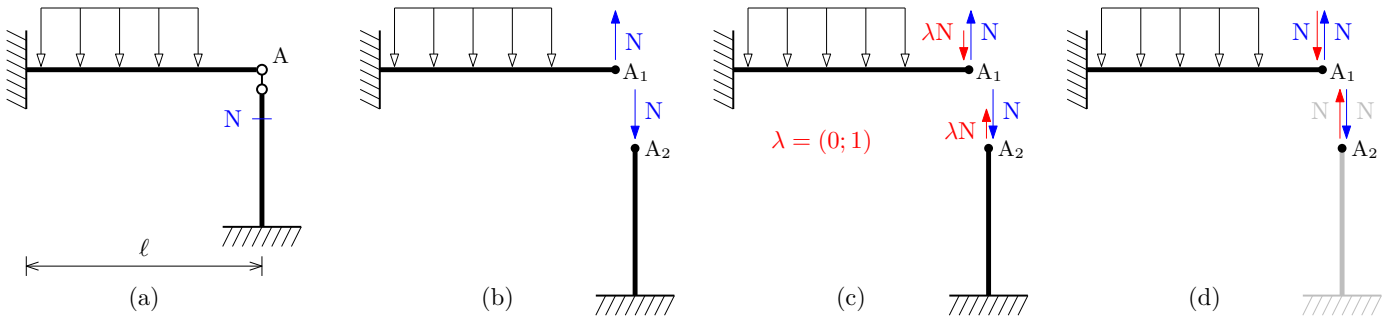

Figure 1: Sequence for modeling the removal of the vertical rod: (a) the axial (compressive) force is computed, (b) Structure 1 and 2 are created and the internal axial force is added as extra nodal force on nodes A_1 and A_2, (c) progressively increasing forces are added on the nodes, (d) the column is removed.

"damaged". It is now interesting to study how the internal energy changes from the undamaged to the damaged situation. With reference to the undamaged structure sketched in Figure 1.a, subjected to an uniformly distributed load q, remembering Clapeyron's theorem, the internal energy is

$$U_0 = \frac{1}{2}\int_{\mathcal{S}} qv\,(z)\,dz, \tag{5}$$

i.e., half the integral over the entire structure $\mathcal{S}$ of the force qdz times the displacement in the undamaged structure $v_0\,(z)$, with z a linear coordinate along the structure. The expression can be rearranged introducing the term

$$C_0 = \frac{\int_{\mathcal{S}} v_0\,(z)\,dz}{q\ell^2} \tag{6}$$

which stands as a compliance term [37]. Thus, Eqn. (5) turns into

$$U_0 = \frac{1}{2}q^2\ell^2 C_0 \tag{7}$$

As expected from the previous discussion, the internal energy for the scheme of Figure 1.b is still U_0 since the forces N perform equal, but opposite, works. When the forces λN are progressively applied, Figure 1.c, mutual works are created. With reference to Figure 1.d, the work from the undamaged (0) to the damaged (d) state is

$$U_{0\to d} = q^2\ell^2\,(C_d - C_0) - \frac{1}{2}N\,(v_{A_1 d} - v_{A_1 0}) - \frac{1}{2}Nv_{A_2 0}. \tag{8}$$

where tthe terms $v_{A_1 0}$ and $v_{A_1 d}$ relate to the vertical displacements of point A_1 in the undamaged (Figure 1.a) and damaged (Figure 1.d) schemes, respectively. Similar nomenclature holds for the vertical displacements of point A_2.

To further simplify Eqn. (8), consider the structure $\mathcal{S}_1$, as depicted in Figure 2. Applying Betti-Maxwell theorem, it results that

$$q^2\ell^2\,(C_d - C_0) = Nv_{A_1 d}. \tag{9}$$

Substituting the left hand-side term of Eqn. (9) equality into Eqn. (8) and remembering that $v_{A_1 0} = v_{A_2 0}$, the following expression of the increment of internal energy is obtained

$$U_{0\to d} = \frac{1}{2}q^2\ell^2\,(C_d - C_0)\,, \tag{10}$$

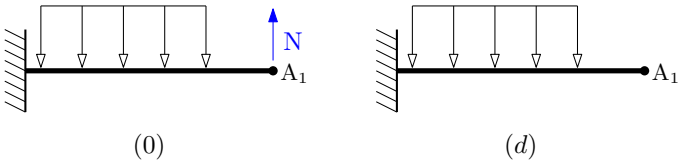

Figure 2: Structure $\mathcal{S}_1$ onto which Betti-Maxwell theorem is applied.

from which the internal energy in the damaged system is

$$U_d = U_0 + U_{0\to d} = \frac{1}{2}q^2\ell^2 C_d. \tag{11}$$

To evaluate the increment of internal energy due to the damage it is sufficient to solve the structure without the damaged element.

Substituting the right hand-side term of Eqn. (9) equality into Eqn. (8), the increment of internal energy turn out to be equal to

$$U_{0\to d} = \frac{1}{2}Nv_{A_1 d}, \tag{12}$$

i.e., larger than the internal energy in the damaged element before the removal ($U_{02} = \frac{1}{2}Nv_{A_1 0}$, with $v_{A_1 0} < v_{A_1 d}$). This means that the deformability of the structure after element removal defines the increment on internal energy.

3. Column removal on a simple frame structure

A simple example is proposed to highlight the parameters that rule the change in internal energy in an elastic frame subjected to element removal. The study case is represented by a one storey five columns frame, as depicted in Figure 3. Column height and beam length are h and ℓ, respectively. The column has cross-section area and inertia A_c and I_c, respectively, and Young's modulus E_c. Similarly, beams are characterized by inertia I_b and elastic modulus E_b. In the following discussion, the quantities EA_c, EI_c and EI_b are considered and the subscript condensed. Vertical downward loads act on the top nodes.

Damage is simulated through the removal of the middle column (in red in Figure 3). To determine the internal energy in the structure after the removal, the symmetry of the damaged

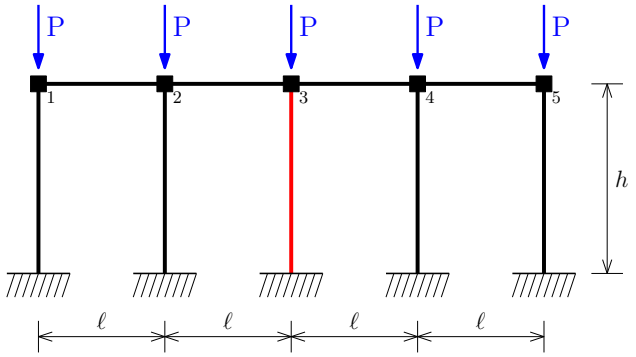

Figure 3: Simple frame structure.

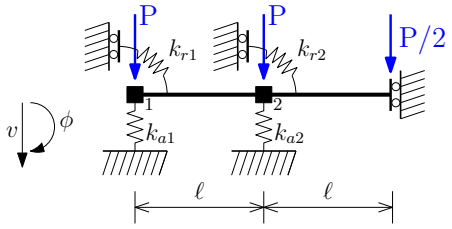

Figure 4: synthetic structural scheme of the damaged frame structure. The squares identify the nodes.

system is considered. Thus, half structure, i.e., the scheme reported in Figure **??**, is studied and its internal energy is doubled. To further simplify the problem, only the top beam is considered. Two allowed displacements are considered for each node: rotational and vertical. The horizontal nodal displacements are not considered in the present analysis since the magnitude of the axial forces in the beams is negligible and, thus, the axial elongations are close to zero. The contribution of each column can be condensed into two springs: a rotational spring having rotational stiffness k_r and a vertical springs having stiffness k_a. In general, such stiffnesses depend on the inertia and the cross-section area of the columns. For the i-th node, it results

$$k_{ri} = \alpha_i \frac{EI_c}{h} \qquad k_{ai} = \beta_i \frac{EA_c}{h} \tag{13}$$

where α_i and β_i depend on the bottom support condition; the subscript $_i$ serves for identifying the node. Figure 4 illustrates the simplified scheme. In the present analysis it results $\alpha_i = 4$ and $\beta_i = 1$ for $i = 1, 2$.

According to the displacement method for structural analysis [55], the following equilibrium equations can be written

$$\begin{cases} \left(\dfrac{4EI_b}{\ell} + k_{r1}\right)\phi_1 + \dfrac{2EI_b}{\ell}\phi_2 + \dfrac{6EI_b}{\ell^2}v_1 - \dfrac{6EI_b}{\ell^2}v_2 = 0 \\ \dfrac{2EI_b}{\ell}\phi_1 + \left(\dfrac{5EI_b}{\ell} + k_{r2}\right)\phi_2 + \dfrac{6EI_b}{\ell^2}v_1 - \dfrac{6EI_b}{\ell^2}v_2 = -P\dfrac{\ell}{4} \\ \dfrac{6EI_b}{\ell^2}\phi_1 + \dfrac{6EI_b}{\ell^2}\phi_2 + \left(\dfrac{12EI_b}{\ell^3} + k_{a1}\right)v_1 - \dfrac{12EI_b}{\ell^3}v_2 = P \\ -\dfrac{6EI_b}{\ell^2}\phi_1 - \dfrac{6EI_b}{\ell^2}\phi_2 - \dfrac{12EI_b}{\ell^3}v_1 - \left(\dfrac{12EI_b}{\ell^3} + k_{a2}\right)v_2 = \dfrac{3}{2}P \end{cases} \tag{14}$$

The first and the second equations refer to the moment equilibrium of nodes 1 and 2, respectively; the third and the fourth to the vertical forces equilibrium of nodes 1 and 2, respectively.

For a regular frame, four dimensionless quantities can be determined rearranging the equations

$$\rho = \frac{EI_b\, h}{EI_c\, \ell} \tag{15}$$

$$\xi = \frac{EA_c\, \ell^2}{EI_c} \tag{16}$$

$$\mu = \frac{P\ell^2}{EI_b} \tag{17}$$

$$\delta_i = \frac{v_i}{\ell} \tag{18}$$

These are obtained by multiplying the first and the second equations times ℓ/EI_b, the remaining times ℓ^2/EI_b and remembering the identity $(\ell EI_c)/(\ell EI_c)$. Parameter ρ is a dimensionless parameter representing the ratio between beam-to-column flexural stiffnesses, ξ is the dimensionless transposed-to-proper column inertia, μ is the dimensionless load and δ the dimensionless vertical displacement. Civil engineering concrete frame structures are characterized by ρ ranging from 0.1 to 10, while ξ larger than 10.

It can be proven that the solution of the system of equations can be expressed as a function of the parameters that defines the shape and the distribution of stiffnesses on the frame and on the terms α_i and β_i that describes the contribution of the condensed columns. In general, the solutions have the form

$$\phi_i = \mu\rho f_{\phi_i}\left(\rho, \xi, \alpha_j, \beta_j\right) \tag{19}$$

$$\delta_i = \mu\rho f_{\delta_i}\left(\rho, \xi, \alpha_j, \beta_j\right) \tag{20}$$

with $j = 1, 2$, where f_ϕ and f_δ are multiplying terms that, in general, depend upon ρ, ξ and on the αs and βs. Referring to the top beam, the bending moment, which varies upon the considered point described through the variable z, is

$$M_b(z) = \frac{EI_b}{\ell}\mu\rho\, m_\phi\left(z, \rho, \xi, \alpha_j, \beta_j\right) + \frac{EI_b}{\ell^2}\mu\rho\left[\ell m_\delta\left(z, \rho, \xi, \alpha_j, \beta_j\right)\right] + P\ell\, m_P(z), \tag{21}$$

where m_ϕ, m_δ and m_P are dimensionless functions that describe the bending moment associated to the rotations, to the displacements and to the external forces, respectively. The term into the square brackets is the (true) displacement of the nodes and $P\ell$ can be rewritten as $\mu\frac{EI_b}{\ell}$. The internal elastic energy associated to the bending moment is

$$U_m = \frac{1}{2}\int_S \frac{[M_b(z)]^2}{EI_b} dz, \tag{22}$$

where the integral is extended over the entire beam. The U_m can be rewritten as

$$U_m = \frac{1}{2}\left(\frac{EI_b}{\ell}\mu^2\right)L_m, \tag{23}$$

where $L_m = L_m\left(\rho, \xi, \alpha_j, \beta_j\right)$ denotes the definite integral and is a scalar quantity dependent upon the dimensionless structural parameters.Referring to the energy in the rotational springs, it is possible to compute

$$U_{k_r} = \frac{1}{2}\sum_{i=1}^{2} k_{ri}\phi_i^2 = \frac{1}{2}\frac{EI_c}{h}\mu^2\rho^2\sum_{i=1}^{2}\beta_i f_{\phi_i}^2. \tag{24}$$

Rearranging the dimensionless quantities, U_{k_r} turns into

$$U_{k_r} = \left(\frac{EI_b}{\ell}\mu^2\right)\rho K_r. \tag{25}$$

where $K_r = K_r\left(\rho, \xi, \alpha_j, \beta_j\right)$ stands for the summation of Eqn. (24). Similarly, the elastic energy in the vertical springs can be computed as

$$U_{k_a} = \frac{1}{2}\sum_{i=1}^{2} k_{ai}v_i^2 = \frac{1}{2}\frac{EA_c}{h}\mu^2\rho^2\ell^2\sum_{i=1}^{2}\beta_i f_{\delta_i}. \tag{26}$$

Similarly, the elastic energy in the vertical springs is

$$U_{k_a} = \frac{1}{2}\left(\frac{EI_b}{\ell}\mu^2\right)\xi\rho K_a \tag{27}$$

where $K_a = K_a\left(\rho, \xi, \alpha_j, \beta_j\right)$ is the summation of Eqn. (26).

Considering the symmetry, the total internal energy after element removal (the so-called damaged structure) is twice the sum of the three contributions

$$U_d = \left(\frac{EI_b}{\ell}\mu^2\right)\left[L_m + \rho K_r + \xi\rho K_a\right]. \tag{28}$$

Adopting the dimensionless quantities, the internal energy of the undamaged structure, Eqn. (**??**) can be rewritten as

$$U_0 = \frac{5}{2}\left(\frac{EI_b}{\ell}\mu^2\right)\frac{\rho}{\xi} \tag{29}$$

The increment $(U_d - U_0) = U_{0\to d}$ of the total energy depends on the geometric quantities ρ and ξ and on the term $\frac{EI_b}{\ell}\mu^2$, which acts as a scaling parameter since it sets the value of the flexural stiffness, the size of the frame and the magnitude of the loads. To generalize, the same conclusions can be drawn even if the span of the beams varies from beam to beam and interstory drift changes from level to level. Similarly, non homogeneous loading on the structure allows to consider that the total energy depends on ρ, ξ and $\frac{EI_b}{\ell}\mu^2$. In fact, a reference length ℓ^*, a reference height h^* and a reference load P^* must be introduced in such a way that beam lengths are all related to their reference values. Similar approach holds for height and loads.

4. Energy redistribution patterns in damaged frames

It was proved that the analysis of two separate structures, the damaged and the undamaged, let to determine the increment of internal energy that occurs in an element removal process on a linear elastic frame. Besides, it results that the increment depends upon geometrical quantities that determine the "shape" of the structure and upon a scaling quantity. Comparing undamaged and damaged schemes, the differences refer to the geometrical quantities, since the scaling terms are kept equal.

Since the increment in internal energy $U_{0\to d}$ is positive, it is interesting to study how the increment is distributed across the entire scheme, if it only affects certain elements, or if a diffused behavior is recorded. Obviously, it is expected that a budget between increases and decreases occurs, i.e., if there are elements in which there is a decrease of internal energy, by consequence, other elements would record larger increments. To study how the energy is redistributed across the scheme, to each element the following dimensionless quantity is assigned

$$\chi_i = \frac{U_{d,i} - U_{0,i}}{U_d - U_0}, \tag{30}$$

where index i denotes each element of the damaged structure (the removed element is not considered), $U_{d,i}$ and $U_{0,i}$ are the internal energies in the i-th element in the damaged and undamaged structure, respectively. Such values can be computed from the internal forces. As $U_d = \sum_i U_{d,i}$ and $U_0 = \sum_i U_{0,i}$, it results that $\sum_i \chi_i = 1$. The term χ is a measure of the contribution of the element with respect to the whole increment of internal energy. If $\chi > 0$, the element accumulate energy, while a loose is seen for $\chi < 0$. For $\chi \approx 0$, i.e., $U_{d,i} \approx U_{0,i}$, no changes are observed.

Tests are performed on a 20 storey 21 columns (420 elements, in total) plane frame structure subjected to vertical downward top loads sketched in Figure 5. For sake of clarity, interstory height h is set equal to beam length ℓ, thus a square nodal grid is generated. Damages consist in column removal; due to the simplicity of the structure in terms of force transfer [44], vertical columns act as load paths and, thus, the removal of a beam does not make any change in load transfer. Four possible damage locations are identified (the red numbers). These are: case 1 (column I-11, central bottom column), case 2 (column I-3, lateral bottom column), case 3 (column X-11, central middle column), case 4 (column X-3, lateral middle column). As χ is a ratio between energies, the scaling terms simplify, thus it results $\chi_i = \chi\left(\rho, \xi, i\right)$. To remember, ρ and ξ are the beam-to-column flexural stiffnesses and transposed-to-proper column inertia ratios, respectively defined in Eqns. (15) and (16). Various parameters configurations were studied: ρ in the range 0.001 to 1000, i.e., from weaker beam-stiffer column to stiffer beam-weak column, respectively; ξ in the range 0.001 to 1000, i.e., from large to small inertia keeping the cross-section area fixed.

Two types results are reported within this section. Figure 6 shows two identical structures subjected to the removal of the central bottom column, Case 1 with $(\rho; \xi) = (1; 10)$. The left-hand side plot depicts the values of χ_i are associated to each element. To highlight increments and reductions, two color scales are adopted: green-to-blue elements are those which experience increments in the internal energy, pink-to-yellow elements record reductions in internal energy. In the following each plot would have its color-scales. Black narrow lines relate to the elements for which $-10^{-3} \leq \chi \leq 10^{-3}$, i.e., those for which no changes are observed. The right-hand side plot summarizes the results depicting, in red color, those elements in which there is

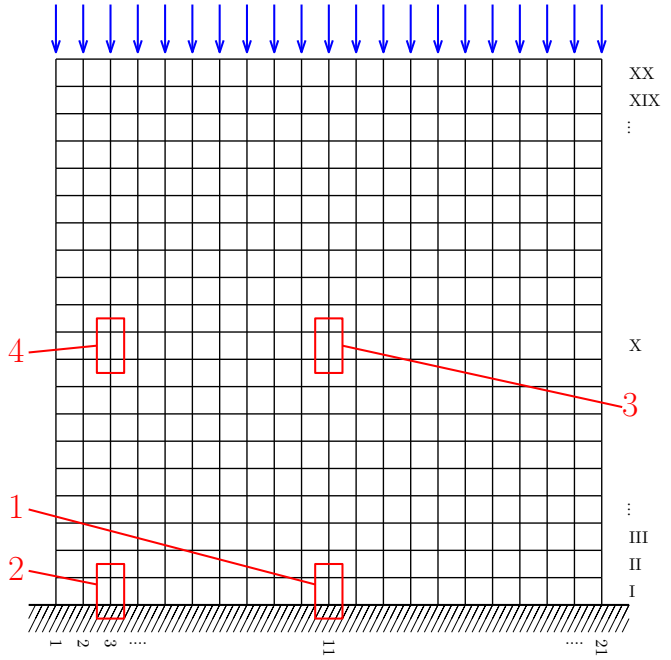

Figure 5: Sketch of the test structure. The vertical alignments of the columns are marked with Arabic numerals (1 to 21), the levels with Roman numerals (I to XX). The removed elements are identified with the red rectangles. The vertical loads are applied on the top of the structure, only.

an increase internal energy. Green elements the ones into which a reduction is observed (the internal energy is still positive, but smaller than in the undamaged case). All the calculations were performed with a Matlab script recalling OpenSees solver [56].

4.1. Case 1: central bottom column

Figure 7 reports the sign of the variation of internal energy into the frame structure subjected to the removal of the central bottom column (Case 1). Each row of the matrix plot of Figure 7 refers to a value of ρ, each column to a value of ξ. A strong influence between ρ, ξ and the sign patterns of χ over the structure after the removal of the central bottom column emerges.

It is first highlighted that an increase of the internal energy (red elements) occurs in the surrounding columns and a reduction (green elements) is in general observed in the columns above the removed element. The variations are not limited to columns, but, to a lesser extent, also to the beams. The extent of the variations largely depends on the values of the dimensionless parameters ρ and ξ, as discussed in the following. Recalling the idea that after element removal there is a sort of energy influence area due to frame redistribution mechanism in which some components are subjected to smaller or larger forces, thus, strain energy, the trends that emerge are the results of two opposite macro-behaviors, as described below.

Referring to parameter ξ, its increment tends to tighten and rise the effects, i.e., the influence area, in term of energy variations due to column removal across the storeys. Fixing a value of ρ, say 0.001, and comparing the plots for low and large ξ, i.e., scrolling the matrix plot of Figure 7 along the rows, it clearly results that the patterns in column energy increments (in red) differs. For low ξ, the increments are seen across all the columns in the bottom levels, while for large ξ the affected columns are those between the alignment of the removed vertical element. Referring to elements in which energy increments are seen are similar: increasing ξ the effect propagates upwards and the influence area tends to close. The same pattern can be seen for the other values of ρ, i.e., along the rows of the matrix plot of Figure 7. In general the number of affected beams increases as much as ξ increases, while their position tends to be across the alignment of the removed column.

On the contrary, referring to parameter ρ, its increase tends to enlarge and flatten the influence area. Similarly to as before, fixing a value of ξ, say 10, and comparing the plots for low and large ρ, that is scrolling the matrix plot of Figure 7 along the columns, it clearly emerges that the location of the elements into which the variation is recorded tends to stretch from the alignment of the removed column. As a second effect, the locations of the affected elements rearrange towards the bottom of the frame, where the removed element was placed.

Such behaviors can be explained recalling that beams are able to laterally redistribute the loads carried by the removed element to the adjacent columns. The stiffer the beam, the more laterally the load is transferred. Transfer beams promote such load paths homogenization across all the columns. The parameter ρ controls such transfer capacity, with larger values implying larger lateral load redistribution. The stiffness of the column arrangement is handled by parameter ξ. Large values imply larger contribution to the whole inertia of the set of columns rather than of the single vertical element. Large ρ and ξ mean a system of rigid beams (with respect to flexure) connecting large columns. Small ρ and large ξ relate to a system into which large columns are connected by weak beams. Large ρ and small ξ reflect a system with rigid beams lying on weak columns.

The last point can be related to the typical case of a frame with deep beams that are able to transfer the loads to the safe elements when a column is removed. In this case, as much as the loads are laterally redistributed, energy increments on each column are smaller since there is a larger diffusion, i.e., the increment is allocated more homogeneously. To better highlight such phenomenon, the colored plots of Figure 8 depict the values of χ_i through the two color ranges previously illustrated. Briefly, the same color means similar energy variation. With reference to the aforementioned case, i.e., $\rho = 1000$ and $\xi = 0.001$ one notes that the bottom columns are green colored ($\chi \approx 0.047$), while those on the second level are in blue ($\chi \approx 0.005$). This does not occur, for example, for $\rho = 10$ and $\xi = 0.001$, where a transition in the colors of the columns is observed.

Analyzing the case in which $\rho = 1000$ and $\xi = 1000$ in Figure 7, an interesting behavior emerges: side columns are subjected to a reduction in internal energy, while central columns to an increase. Insights on such behavior can be explained observing the same configuration in Figure 8: it comes out that the inner bottom columns are subjected to an increase, the external to a decrease and the ones in-between to a null increment. Since

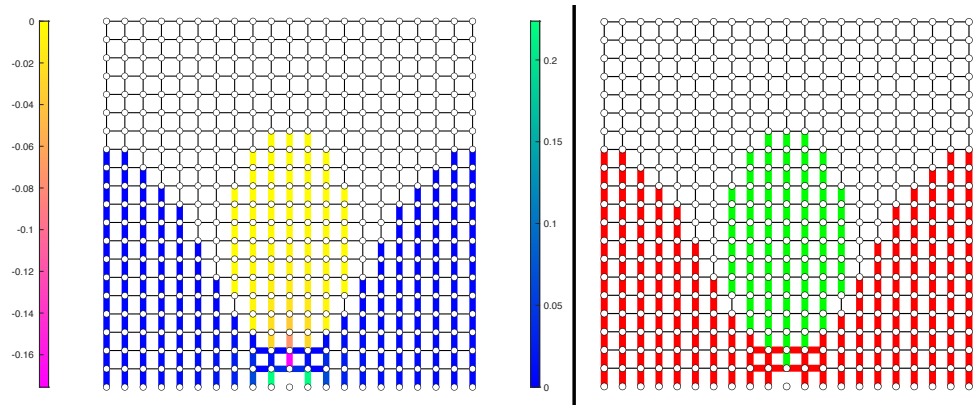

Figure 6: Sample plots aiming at presenting the results. The structures have equal ρ and ξ and are subjected to the same damage. Referring to the left-hand side plot: the values of χ are presented and two colorbars are adopted: green-to-blue colorbar relates to internal energy increments, pink-to-yellow to internal energy reductions. Referring to the right-hand side plot: the increment or decrement is highlighted, only: red elements experience internal energy increment while green elements experience internal energy reduction. In both plots black narrow lines relate to elements into which the increment is negligible.

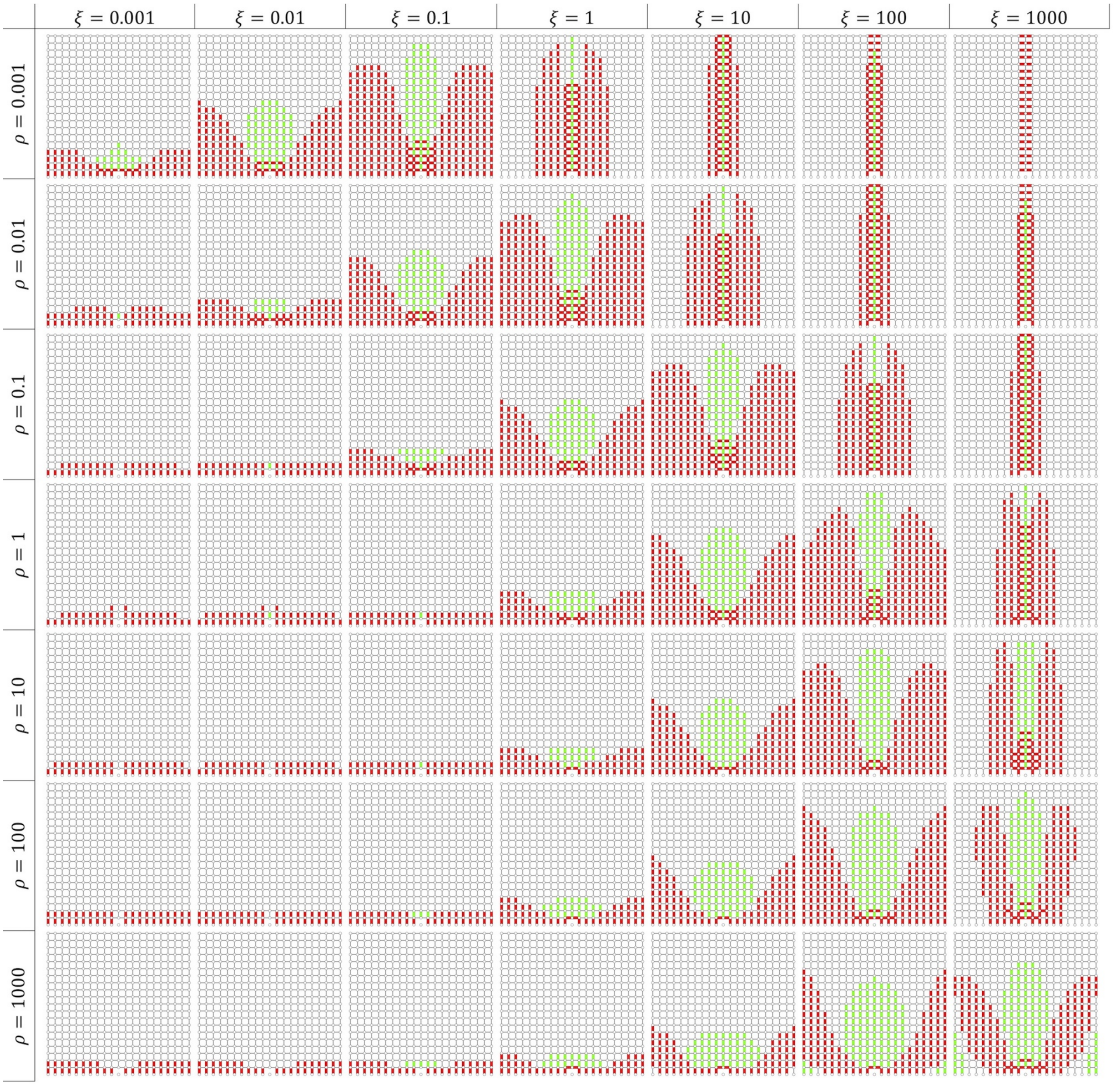

Figure 7: Patterns of internal energy variation following the removal of the central bottom column (Case 1 of Figure 5). The color of the elements relates to the variation in the internal energy. Red elements have $\chi > 10^{-3}$, green elements have $\chi < -10^{-3}$, black elements are those for which $|\chi| < 10^{-3}$.

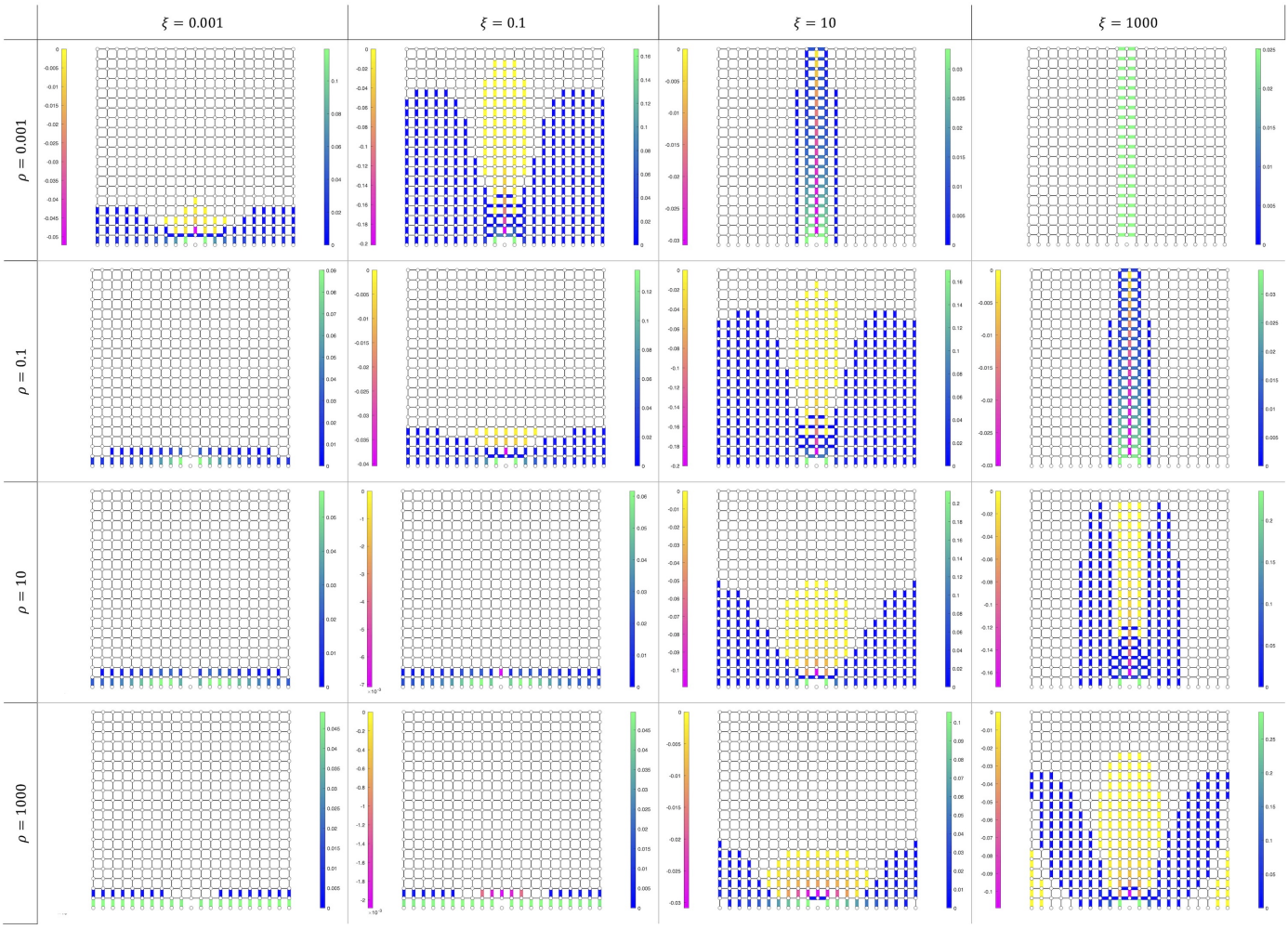

Figure 8: Values of χ, defined in Eqn. (30) for various pairs of ρ and ξ. The value of the ratio is reported if $|\chi| > 10^{-3}$. Each structure has two colorbars: the right-hand side green-to-blue colorbar relates to increments of internal energy, i.e.,$\chi > 10^{-3}$; the left-hand side pink-to-yellow colorbar relates to reductions of internal energy, i.e., $\chi < -10^{-3}$.

such elements are quasi-exclusively subjected to an axial force, this can be traced back to a flexural sectional behavior with a fictitious neutral axis representing the null energy increment.

The plots of Figure 8 details that, in general, the larger local energy variations occur in those elements that are close to the removed column. A uniform variation is observed when the homogeneous behavior is achieved, i.e., for very small ρ and very large ξ, or viceversa.

Finally, comparing the whole matrix it can be noted that similar color pattern clearly emerges for different $(\rho;\xi)$ pairs. For example, there are similitudes between the plots at (0.001; 0.01), (0.01;0.1), (0.1;1), and at (10;10). It can be stated that similar increase/decrease patterns (green/red columns) are seen for $\xi \approx 10\rho$ for $\rho \leq 0.1$.

4.2. Case 2: lateral bottom column

The patterns in terms of energy increment and decrements that originate in the structure when subjected to the removal of a bottom side column are reported in Figure 9. The mutual opposite contribution of ρ and ξ highlighted for Case 1 similarly emerges. What is herein interesting is the presence on the frame of parts that experience a reduction of strain energy, and others that are subjected to energy increments. Although the damage is located on the side of the frame, the effects extend to the opposite site. Also in this damage case, there are parts of the structure in which there are no variations, surrounded by parts in which increase or reductions are observed. This proves that there is a sort of energy compartmentalization [57] for which, on one side, there are components that are not affected, while others are subjected to the effects of the damage. The mutual contribution of the stiffness of the beams and the stiffness of the arrangements of columns determine a different lateral diffusion of the patterns across the various levels of the frame structure. This aspect clearly appear, for example, at $(\rho;\xi) = (1000; 100)$: certain columns experience, at the bottom levels, lesser energy, while the same columns at the higher levels are subjected to energy increases.

As already noted for the middle bottom column removal, analogies in the patterns are seen across the matrix plot of Figure 9. It can be stated that similar increase/decrease patterns (green/red columns) are seen for $\xi \approx 10\rho$ for $\rho \leq 1$. For larger ρ, the patterns turn to be roughly independent from the value of ξ, meaning that the contribution of columns assembly is somehow negligible.

4.3. Cases 3 and 4: central and lateral middle columns

Figures 10 and 11 detail the patterns that originate in the structure when the central (Case 3) or lateral (Case 4) columns at frame mid-height are removed. It is noted that the counterposing contribution of the two parameters still emerges in such damage cases. Briefly, the increase of parameter ρ implies a narrower and taller extent of the influence area, while the opposite effect is achieved by increasing parameter ξ. Horizontal symmetric patterns are clearly highlighted on Case 3. In general, the effects of column removal can be summarized as follow. (i) Below and above the removed column, an area of energy reduction is always observed. In the ultimate case, the reduction involves the upper elements, only, of the damaged column alignment. (ii) Energy increases are, on the contrary, observed on the sides of the damaged element. The damage, in some cases, can have effects on the whole frame, as observed in $(\rho;\xi) = (0.1; 10)$ of Figure 10. For the majority of the examined cases, the effects propagates along the vertical and horizontal directions. For $\xi = 1000$ and $\rho = 0.001$, i.e, for the ultimate cases, the effects are limited to the upper beams, only. This already emerged in Cases 1 and 2 previously analyzed.

It is interesting to note that, in some cases, there are parts of the structure located far from the damaged element into which energy reduction is observed. This is clearly visible, for example, in the removal of the side column (Case 4) for those structures for which $\xi = 100$ and $\rho \geq 1$. As already emerged for the previously analyzed cases, there are patterns that are similar along the top-left bottom-right diagonal of both matrix plots, i.e., for $\xi \approx 10\rho$.

5. Discussion

The patterns that have been highlighted show the complexity of frame behavior. Recalling the theoretical results presented in Section 2, the damage always implies an increment in the internal energy. The analysis on the simple frame structure highlights that there are relevant dimensionless quantities that govern the behavior of the frame and, thus, the internal energy once loaded. Dimensionless quantities are at the base of the dimensional analysis approach that follows from Buckingham's Π-theorem [58]. Following Buckingham's Π-theorem, the total number of dimensionless quantities that serve for describing the system it would be four. This results considering ℓ and EI_b as repeating terms and, thus, creating four dimensionless quantities for the remaining variables, i.e., h, EI_c, A_c and P. The additional findings on structural behavior proved that the effective number of dimensionless quantities is three (ρ, ξ and μ).

Besides the previous consideration, the total energy increase after element removal, i.e., $U_{0\to d}$, is a measure of the ability of the structural system to support with limited displacements the applied loads. The dimensionless increment can be evaluated through a parameter R, as

$$R = \frac{U_d - U_0}{U_0} \tag{31}$$

The value R depends on the location of the removed element, the size of the frame and on ρ and ξ. Figure 12 depicts the values of R for various pairs $(\rho;\xi)$ that originates when the middle bottom column is removed. The reader should note that logarithmic scales are adopted for the three axes. The plot highlights that for low ρ and large ξ the ratio is larger than 1, meaning that the total energy in the damaged structure is larger than twice the energy in the undamaged scheme. A saddle-like surface plot emerges, with a hill-like increase for small ξ and $\rho \approx 1$. The maximum R related to this part of the surface is around $10^{-1.81} = 0.0154$. With reference to the simulated structures,

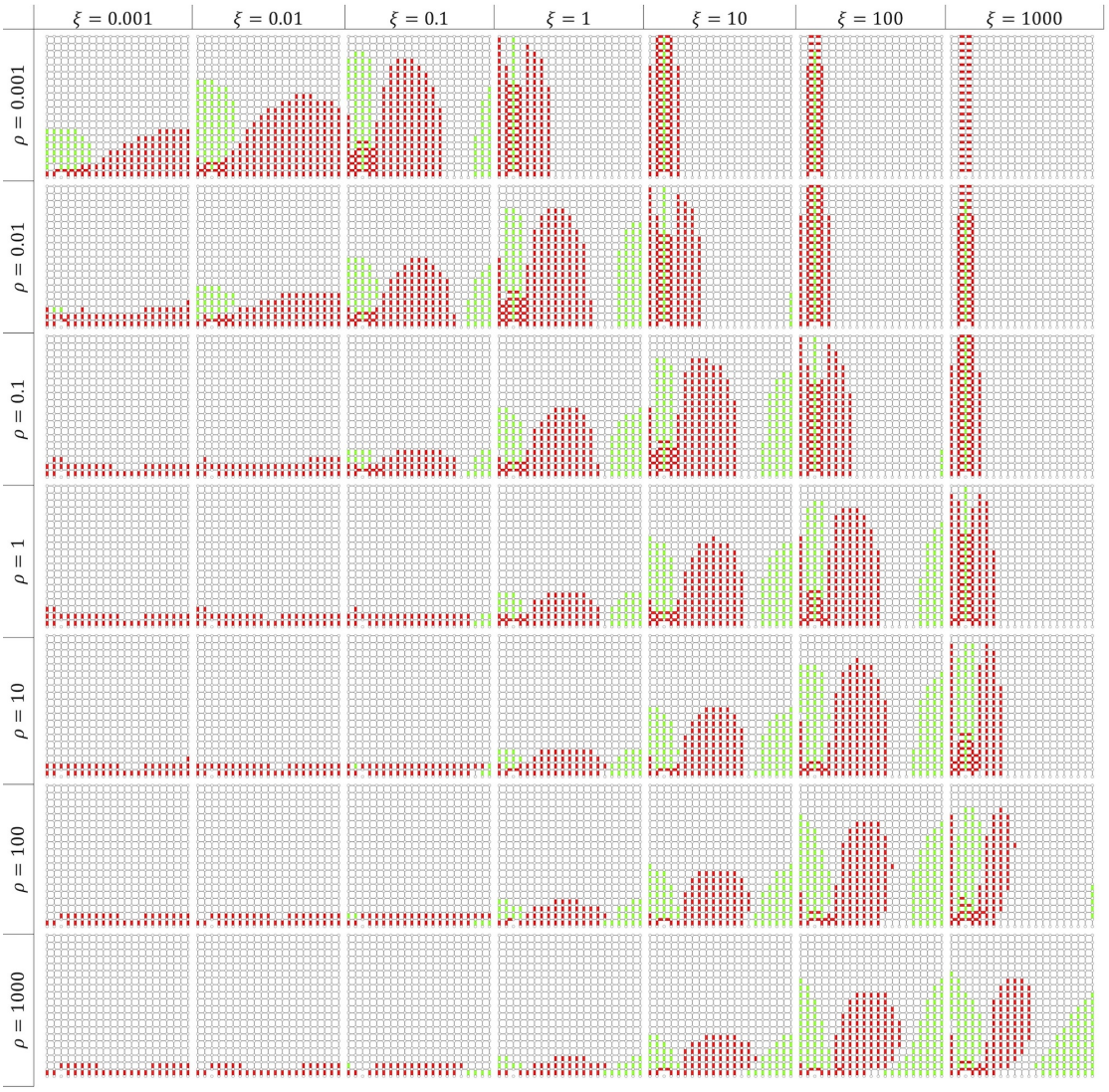

Figure 9: Patterns of internal energy variation following the removal of the lateral bottom column (Case 2 of Figure 5). The color of the elements relates to the variation in the internal energy. Red elements have $\chi > 10^{-3}$, green elements have $\chi < -10^{-3}$, black elements are those for which $|\chi| < 10^{-3}$.

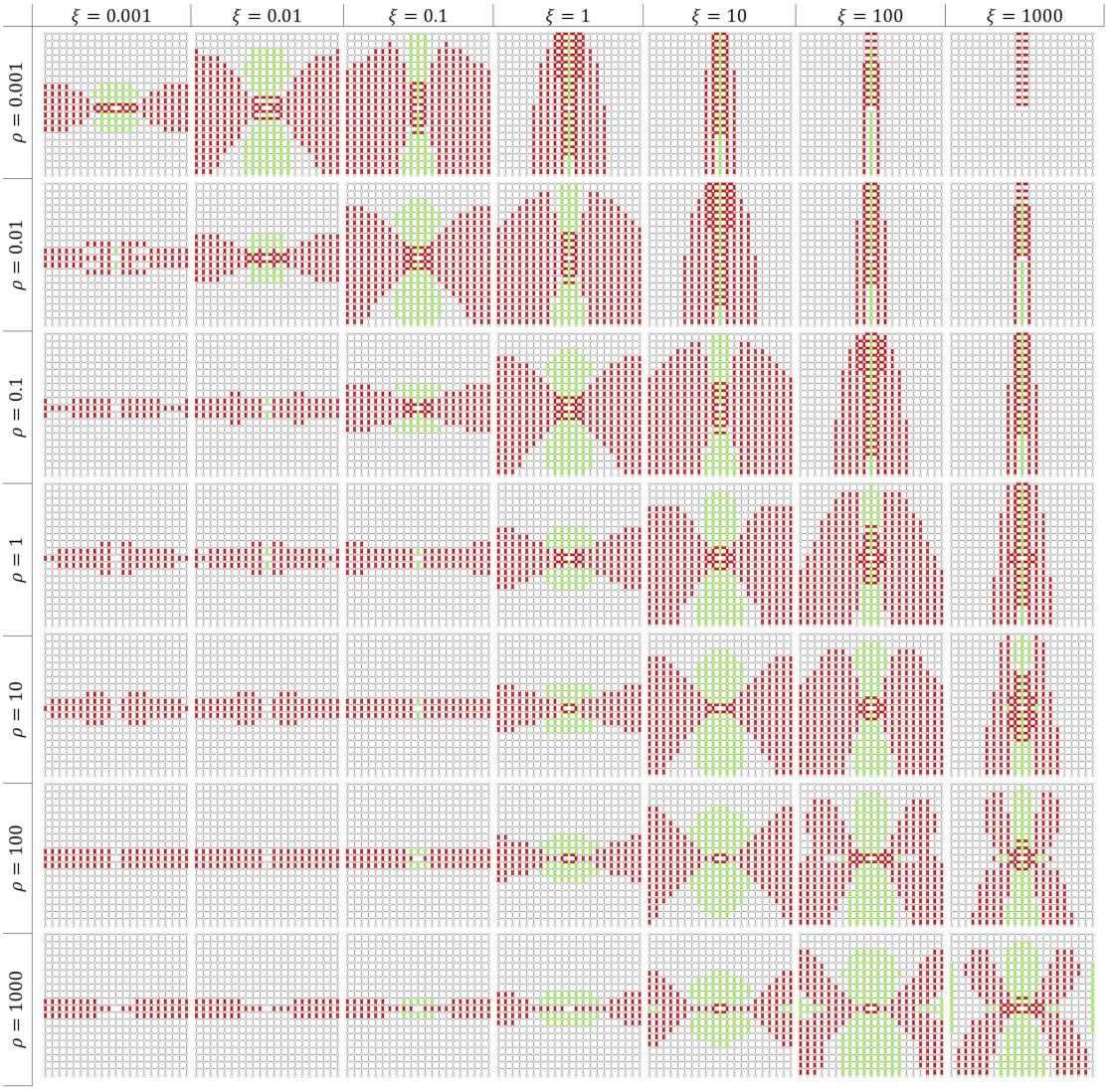

Figure 10: Patterns of internal energy variation following the removal of the central middle column (Case 3 of Figure 5). The color of the elements relates to the variation in the internal energy. Red elements have $\chi > 10^{-3}$, green elements have $\chi < -10^{-3}$, black elements are those for which $|\chi| < 10^{-3}$.

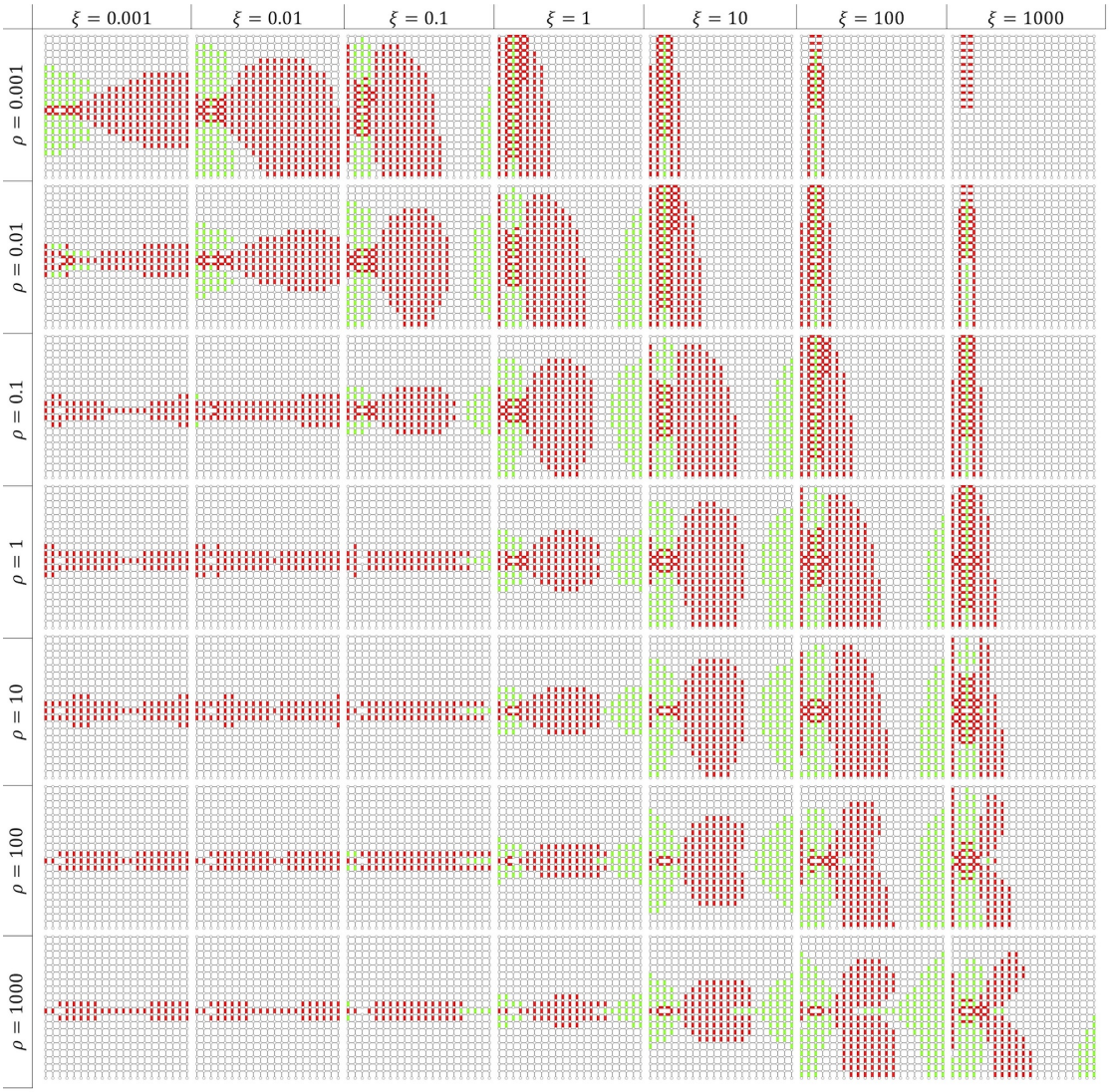

Figure 11: Patterns of internal energy variation following the removal of the central middle column (Case 4 of Figure 5). The color of the elements relates to the variation in the internal energy. Red elements have $\chi > 10^{-3}$, green elements have $\chi < -10^{-3}$, black elements are those for which $|\chi| < 10^{-3}$.

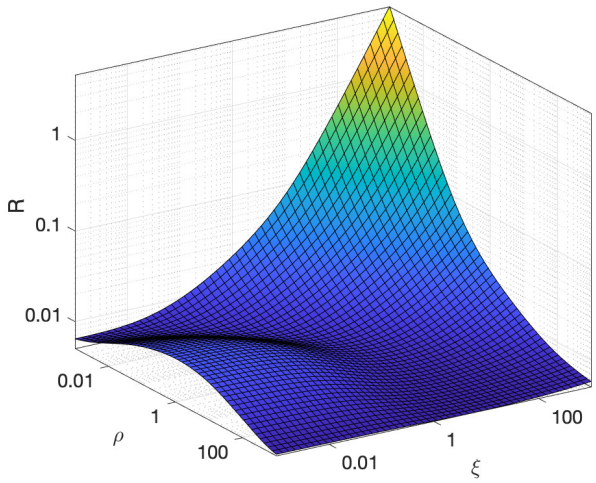

Figure 12: Case 1. Surface plot of the values of the dimensionless energy increment R for various pairs of ρ and ξ. Logarithmic scales have been chosen for the three axes.

the minimum R is observed for the largest ρ, i.e., $\rho = 1000$, and ξ around 10.

With the purpose to relate the increment R and the energy pattern on the frame, the contour plots of the value R for the four cases have been plotted in Figure 13. Due to the large range and the need of highlighting the local behaviors, the contour lines refer to $\log_{10} R$, rather than to R, itself. That is, a value, say, -2, denotes a $R = 10^{-2} = 0.01$. Logarithmic axes have been adopted for ρ and ξ. The shapes previously illustrated, i.e., saddle and hill-like, clearly emerges from the contour lines of the plots. On the background of the plots, Figures 7, 9, 10 and 11 have been sketched. The blue dots mark on the $\rho;\xi$ axes the correct position of the pattern plot onto which they are placed.

It clearly appears that the behavior in terms of R are similar for the four analyzed cases, both in terms of the value of R and in its trend across the various modeled structures. Although more or less evident, the saddle-point of R is located around $(\rho;\xi) = (0.1;1)$. The upper right part of the plot depicts a progressively increasing value of R with a constant trend along the log-log axes plot.

The contour lines divide the $\rho;\xi$ plot into two areas with similar trends: a right-upper part, namely part A, into which the contour lines on the log-log axes are oriented along the minor diagonal (top-left towards bottom-right) with a sharp increase; a left part, namely part B, into which the hill-like shape is observed. The separation line between the two parts can be identified by the lines passing through the following points: $(0.001;0.01) \rightarrow (1;10) \rightarrow (1000;10)$.

Comparing the trends in the contour lines and the similarities between underneath patterns previously highlighted it appears that the structural configurations lying in part A and exhibiting the same R, although different, present the same energy pattern. This does not occur for the structural configurations of part B.

6. Conclusions

The present paper deals with the behavior of a frame structure subjected to column removal. In general, damage always implies a reduction of stiffness and, by consequence, an increase of the internal energy on the system. It was proven that the amount of increment of energy depends on the deformability of the system after element removal and on the internal forces in the removed member before the removal. For linear elastic plane frame structures it was found that there three are relevant dimensionless quantities that govern the deformation and, by consequence, the internal energy of the system once loaded.

Four tests were performed on a 20 storey, 21 columns frame structure subjected to column removal in different location. The modification of the structural scheme caused variation of the internal energy in the frame. Different energy patterns, intended as energy increase or decrease, were highlighted. Analogies in the pattern between different structural configurations were highlighted. This was confirmed in the plots of the dimensionless increment, provided that the dimensionless parameters ρ and ξ describing the distribution of stiffness across the structure fulfill the following inequalities

$$\begin{cases} \xi \geq 10\rho & \text{for } \rho \geq 0.001 \\ \xi \geq 10 & \text{for } \rho \geq 1 \end{cases} \tag{32}$$

The theoretical and numerical analyses herein performed provided an interesting and unusual insight into frame behavior. To generalize the results, a simple comparison between frames with varying beam length or floor height is performed. Figure 14 shows the pattern distribution (positive and negative χ) for a $\rho = 1$, $\xi = 10$ frame structure subjected to central bottom column removal. The four structures are characterized by a double length span (beams between columns 6 and 7) and/or by a double height floor (storey VI). Although the patterns seems to be similar, a slightly variation from structure to structure occurs. The main considerations about the effects of ρ and ξ holds: for ρ increasing, i.e., for a larger h or a lower ℓ, the effects tend to widen and flatten. This is observed comparing Figure 14.a and 14.b. The top green columns are three in (a) case, while only one in (b) case. A symmetrical pattern is present since the change in the structure is symmetrical. On the contrary, for a reducing ρ, for example due to a locally larger beam length, the energy pattern tends to be more narrow and taller. Comparing Figure 14.a and 14.c this clearly emerges: the left part of the structure, the one in which a local increase of ρ is present, shows such effects, which contribution also depends on ξ. An increase of ξ, i.e., larger beam length, produces the same effects as a reduction of ρ. Case (d) of Figure 14 summarizes the two opposite trends. This simple, but effective, example provides a generalization of the findings of the present analyses, showing that a local variation in the geometry of the frame induces a modification of the energy patterns.

The main results of this study would be the base for more accurate analyses taking into account, for example, the patterns that originates when the element is not completely removed,

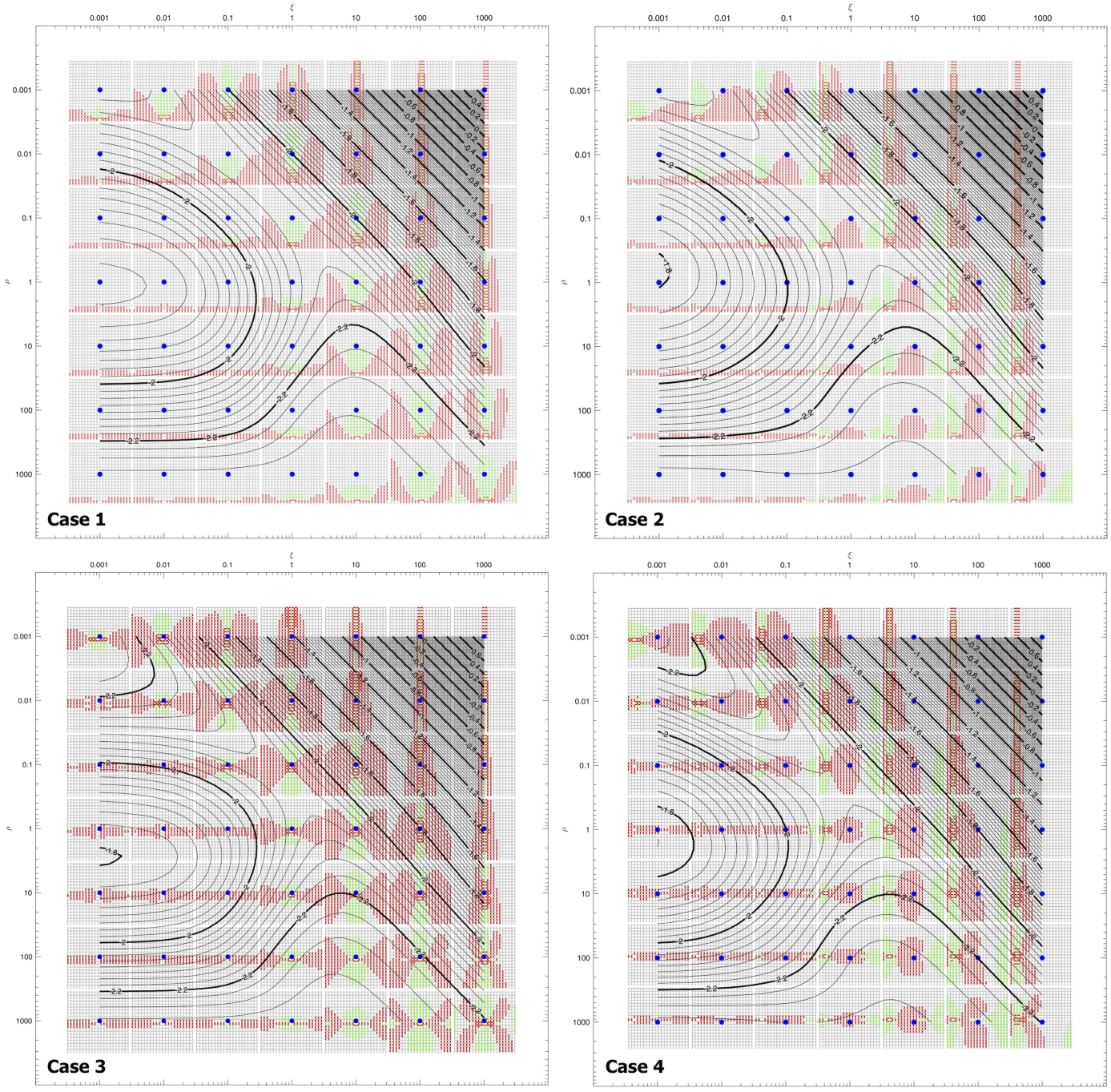

Figure 13: Contour plots of the logarithm of the dimensionless energy increment, $\log_{10} R$, for the four analyzed damage configurations. Logarithmic axes are adopted for the parameters ρ and ξ, defined in Eqns. (15) and (16), as the beam-to-column flexural stiffnesses and transposed-to-proper column inertia ratios, respectively. The saddle-like and hill-like shapes are visible in each plot. In the background of each contour plots the corresponding pattern figure is presented. The blue dots mark, on $\rho;\xi$ axes, the correct position of the pattern plot onto which they are placed.

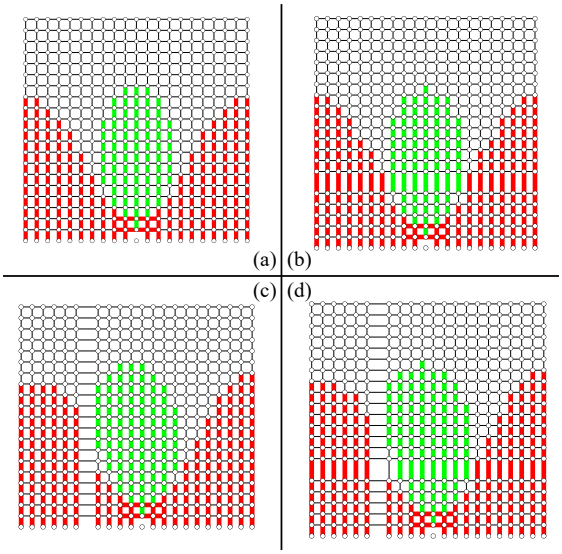

Figure 14: Comparison between four different structures having $\rho = 1$, $\xi = 10$. Structure in (b) is characterized by a a double height floor at storey VI, structure in (c) by a double length span for the beams between columns 6 and 7, while structure in (d) by both geometry variations. Red elements have $\chi > 10^{-3}$, green elements have $\chi < -10^{-3}$, black elements are those for which $|\chi| < 10^{-3}$.

or the possibility of compartmentalizing a frame structure to prevent damage propagation. The findings can be obviously applied to civil structures: knowing the extent of the damage would allow to design damage-tolerant systems. Even if the results hold, in the present stage, for planar frames, it should be remembered that in civil constructions the primary frames, i.e., planar frames, carry dead and live loads, while secondary frames are devoted to support lateral loads. This allows to apply the present results to real civil engineering study cases. Meanwhile, some results could be interesting in the analysis of periodic structures subjected to damage.

References

[1] J. Heyman, Beams and Framed Structures: Structures and Solid Body Mechanics, 2nd Edition, Elsevier, 2013.

[2] K.-G. Olsson, O. Dahlblom, Structural mechanics: modelling and analysis of frames and trusses, John Wiley & Sons, 2016.

[3] G. Ramaswamy, M. Eekhout, Analysis, design and construction of steel space frames, Thomas Telford, 2002.

[4] J. Wu, Q. Li, Structural performance of multi-outrigger-braced tall buildings, The structural design of tall and special buildings 12 (2) (2003) 155–176.

[5] M. M. Ali, K. S. Moon, Advances in structural systems for tall buildings: emerging developments for contemporary urban giants, Buildings 8 (8) (2018) 104.

[6] L. Zhu, N. Li, P. Childs, Light-weighting in aerospace component and system design, Propulsion and Power Research 7 (2) (2018) 103–119.

[7] W. P. Syam, W. Jianwei, B. Zhao, I. Maskery, W. Elmadih, R. Leach, Design and analysis of strut-based lattice structures for vibration isolation, Precision Engineering 52 (2018) 494–506.

[8] L. Wang, M. C. Boyce, C.-Y. Wen, E. L. Thomas, Plastic dissipation mechanisms in periodic microframe-structured polymers, Advanced Functional Materials 19 (9) (2009) 1343–1350.

[9] F. Dadgar-Rad, A. Beheshti, A nonlinear strain gradient finite element for microbeams and microframes, Acta Mechanica 228 (5) (2017) 1941–1964.

[10] T. H. G. Megson, Introduction to Aircraft Structural Analysis, Butterworth-Heinemann, 2013.

[11] M. Rahman, Ultimate strength estimation of ships' transverse frames by incremental elastic–plastic finite element analysis, Marine structures 11 (7-8) (1998) 291–317.

[12] L. Boniotti, S. Beretta, S. Foletti, L. Patriarca, Strain concentrations in bcc micro lattices obtained by am, Procedia Structural Integrity 7 (2017) 166–173.

[13] S. K. Shah, M. Shah, A. Sur, S. Darvekar, Outline of lattice structures: Morphology, manufacturing, and material aspect, in: Advances in Communication and Computational Technology, Springer, 2021, pp. 245–255.

[14] J. Aizenberg, J. C. Weaver, M. S. Thanawala, V. C. Sundar, D. E. Morse, P. Fratzl, Skeleton of euplectella sp.: structural hierarchy from the nanoscale to the macroscale, Science 309 (5732) (2005) 275–278.

[15] FEMA, The oklahoma city bombing: Improved building performance through multihazard mitigation (fema 277), Tech. rep., Washington DC: American Society of Civil Engineers (1996).

[16] N. I. of Standards, Technology, Final report on the collapse of the World Trade Center towers, US Department of Commerce, Technology Administration, National Institute of . . . , 2005.

[17] B. Behnam, Fire structural response of the plasco building: A preliminary investigation report, International Journal of Civil Engineering 17 (5) (2019) 563–580.

[18] J. Agarwal, M. Haberland, M. Holickỳ, M. Sykora, S. Thelandersson, Robustness of structures: Lessons from failures, Structural Engineering International 22 (1) (2012) 105–111.

[19] M. Sasani, Response of a reinforced concrete infilled-frame structure to removal of two adjacent columns, Engineering Structures 30 (9) (2008) 2478–2491.

[20] F. Kiakojouri, V. De Biagi, B. Chiaia, M. R. Sheidaii, Progressive collapse of framed building structures: Current knowledge and future prospects, Engineering Structures 206 (2020) 110061.

[21] F. Kiakojouri, M. Sheidaii, V. De Biagi, B. Chiaia, Progressive collapse assessment of steel moment-resisting frames using static-and dynamic-incremental analyses, Journal of Performance of Constructed Facilities 34 (3) (2020) 04020025.

[22] F. Fu, Progressive collapse analysis of high-rise building with 3-d finite element modeling method, Journal of Constructional Steel Research 65 (6) (2009) 1269–1278.

[23] J. Mashhadi, H. Saffari, Effects of damping ratio on dynamic increase factor in progressive collapse, Steel and Composite Structures 22 (3) (2016) 677–690.

[24] M.-H. Tsai, B.-H. Lin, Investigation of progressive collapse resistance and inelastic response for an earthquake-resistant rc building subjected to column failure, Engineering structures 30 (12) (2008) 3619–3628.

[25] A. H. Arshian, G. Morgenthal, Three-dimensional progressive collapse analysis of reinforced concrete frame structures subjected to sequential column removal, Engineering Structures 132 (2017) 87–97.

[26] C. Grunwald, A. A. Khalil, B. Schaufelberger, E. M. Ricciardi, C. Pellecchia, E. De Iuliis, W. Riedel, Reliability of collapse simulation–comparing finite and applied element method at different levels, Engineering Structures 176 (2018) 265–278.

[27] M. Ebrahimi, R. Karami Mohammadi, Damage detection of steel moment frames under earthquake excitation, Structural Control and Health Monitoring 27 (10) (2020) e2599.

[28] H. F. Lam, C. T. Ng, The selection of pattern features for structural damage detection using an extended bayesian ann algorithm, Engineering Structures 30 (10) (2008) 2762–2770.

[29] R. P. Bandara, T. H. Chan, D. P. Thambiratnam, Frequency response function based damage identification using principal component analysis and pattern recognition technique, Engineering Structures 66 (2014) 116–128.

[30] M.-H. Tsai, An analytical methodology for the dynamic amplification factor in progressive collapse evaluation of building structures, Mechanics Research Communications 37 (1) (2010) 61–66.

[31] V. D. Biagi, F. Kiakojouri, B. Chiaia, M. R. Sheidaii, A simplified method for assessing the response of rc frame structures to sudden column removal, Applied Sciences 10 (9) (2020) 3081.

[32] B. I. Song, H. Sezen, Experimental and analytical progressive collapse assessment of a steel frame building, Engineering structures 56 (2013) 664–672.

[33] S. Gerasimidis, Analytical assessment of steel frames progressive col-

lapse vulnerability to corner column loss, Journal of Constructional Steel Research 95 (2014) 1–9.
[34] K. Qian, B. Li, Quantification of slab influences on the dynamic performance of rc frames against progressive collapse, Journal of Performance of Constructed Facilities 29 (1) (2015) 04014029.
[35] E. Masoero, P. Darò, B. Chiaia, Progressive collapse of 2d framed structures: An analytical model, Engineering structures 54 (2013) 94–102.
[36] P. Pantidis, S. Gerasimidis, New euler-type progressive collapse curves for steel moment-resisting frames: Analytical method, Journal of Structural Engineering 143 (9) (2017) 04017113.
[37] G. Sih, R. Hartranft, The concept of fracture mechanics applied to the progressive failure of structural members, Computers & Structures 12 (6) (1980) 813–818.
[38] B. M. Chiaia, E. Masoero, Analogies between progressive collapse of structures and fracture of materials, International journal of fracture 154 (1-2) (2008) 177–193.
[39] E. Masoero, F. K. Wittel, H. J. Herrmann, B. Chiaia, Hierarchical structures for a robustness-oriented capacity design, Journal of engineering mechanics 138 (11) (2012) 1339–1347.
[40] E. Masoero, F. K. Wittel, H. J. Herrmann, B. Chiaia, Progressive collapse mechanisms of brittle and ductile framed structures, Journal of engineering mechanics 136 (8) (2010) 987–995.
[41] J. Lemaitre, J.-L. Chaboche, Mechanics of solid materials, Cambridge university press, 1994.
[42] V. De Biagi, Structural behavior of a metallic truss under progressive damage, International Journal of Solids and Structures 82 (2016) 56–64.
[43] V. De Biagi, B. M. Chiaia, Damage tolerance in parallel systems, International Journal of Damage Mechanics 25 (7) (2016) 1040–1059.
[44] V. De Biagi, B. Chiaia, Complexity and robustness of frame structures, International Journal of Solids and Structures 50 (22-23) (2013) 3723–3741.
[45] E. G. Karpov, Structural metamaterials with saint-venant edge effect reversal, Acta Materialia 123 (2017) 245–254.
[46] E. G. Karpov, L. A. Danso, J. T. Klein, Anomalous strain energy transformation pathways in mechanical metamaterials, Proceedings of the Royal Society A 475 (2226) (2019) 20190041.
[47] F. Biondini, D. M. Frangopol, S. Restelli, On structural robustness, redundancy, and static indeterminacy, in: Structures Congress 2008: Crossing Borders, 2008, pp. 1–10.
[48] E. Masoero, Casco: a simulator of load paths in 2d frames during progressive collapse, SN Applied Sciences 2 (9) (2020) 1–17.
[49] D. Stephen, D. Lam, J. Forth, J. Ye, K. D. Tsavdaridis, An evaluation of modelling approaches and column removal time on progressive collapse of building, Journal of Constructional Steel Research 153 (2019) 243–253.
[50] V. De Biagi, F. Parisi, D. Asprone, B. Chiaia, G. Manfredi, Collapse resistance assessment through the implementation of progressive damage in finite element codes, Engineering Structures 136 (2017) 523–534.
[51] S. Timoshenko, History of strength of materials: with a brief account of the history of theory of elasticity and theory of structures, Courier Corporation, 1983.
[52] A. P. Boresi, R. J. Schmidt, O. M. Sidebottom, et al., Advanced mechanics of materials, Vol. 6, Wiley New York, 1993.
[53] G. Colonnetti, Statica delle costruzioni, volume 1, UTET, Torino, 1928.
[54] M. H. Sadd, Elasticity: theory, applications, and numerics, Academic Press, 2009.
[55] I. A. Karnovsky, O. Lebed, Advanced methods of structural analysis, Springer Science & Business Media, 2010.
[56] F. McKenna, M. H. Scott, G. L. Fenves, Nonlinear finite-element analysis software architecture using object composition, Journal of Computing in Civil Engineering 24 (1) (2010) 95–107.
[57] C. Cennamo, B. Chiaia, V. De Biagi, L. Placidi, Monitoring and compartmentalized structures, ZAMM-Journal of Applied Mathematics and Mechanics/Zeitschrift für Angewandte Mathematik und Mechanik 95 (6) (2015) 638–648.
[58] G. I. Barenblatt, G. I. Barenblatt, B. G. Isaakovich, Scaling, self-similarity, and intermediate asymptotics: dimensional analysis and intermediate asymptotics, Vol. 14, Cambridge University Press, 1996.